

**Practical Aspects of Calibrating Near-Infrared Interferometer
Data: Predicting Stellar Angular Sizes**

Gerard T. van Belle

Jet Propulsion Laboratory, California Institute of Technology,
4800 Oak Grove Drive, Pasadena, CA 91109

Received _____; accepted _____

ABSTRACT

Reliable prediction of stellar diameters, particularly angular diameters, is a useful and necessary tool for the increasing number of milliarcsecond resolution studies being carried out in the astronomical community. Specifically, the task of calibrating visibility amplitude information from astronomical interferometers often requires the ability to reliably estimate diameters and uncertainties associated with those diameters. The approaches generally used throughout the literature are discussed and compared. Predictions from assumptions of stellar linear size and distance are generally poor, while fitting these objects as blackbody radiators is a better approach, with certain limitations discussed herein. A relatively accurate technique of predicting $V = 0$ and $B = 0$ apparent angular sizes is presented for both giant and supergiant stars, and for more evolved sources. This technique uses observed B , V , and K magnitudes to predict angular sizes for giant and supergiant stars to 22–25% for a 99% confidence level result. Application of these techniques towards the task of normalizing visibilities from interferometers is also discussed in detail.

Subject headings: Instrumentation: interferometers — stars: fundamental parameters — infrared: stars

1. Introduction

In the last 15 years, near-infrared interferometers have evolved from rudimentary prototypes to the first generation of facility instruments, from the first fringes at CERGA (Di Benedetto & Conti 1983) to the Earth-scanned fringes at IRMA (Benson et al. 1991) to the recent near-IR first fringes with NPOI (Dyck 1998a). Prior to the results from long-baseline interferometry, lunar occultations were utilized to measure stellar angular sizes (Ridgway et al. 1977) and continue to provide a steady stream of diameters (Richichi et al. 1998), to which the size determination techniques presented herein are equally applicable.

In interpreting long baseline interferometer data, one is frequently interested in establishing the point-source response of the instrument. This response can be measured by observing calibration sources with the interferometer - sources that are effectively unresolved or close to unresolved by the interferometer, and reliably predicted as such. The calibrator response will be convolved with that of the atmosphere as well as the instrument. Due to the temporal and spatial variations of the atmosphere, calibration sources are desired to be close to the science target(s) in both angle and in time. In this sense, calibration sources are utilized much like standard stars for photometry. Use of calibration sources is well established in the infrared (cf. Di Benedetto 1985, Dyck et al. 1996a) and the visible (cf. Mozurkewich et al. 1991, Baldwin et al. 1996). A detailed investigation of stellar surface brightness as a function of $V - K$ color has already been published by Di Benedetto (1993), building on the previous work by Barnes & Evans (Barnes et al. 1976a, 1976b, 1978), studies that are of course closely related to the question of angular size being addressed by this manuscript.

One of the powerful aspects of interferometric data is the ability to provide precise angular sizes for large stars, even in the presence of large uncertainties for the smaller calibration sources. However, as astronomical interferometers have grown in size (from the

4.8 m baseline of IRMA to the 110m baseline of PTI; cf. Benson et al. 1991, Colavita et al. 1999), ‘unresolved’ sources have become more scarce. The next generation of instruments (e.g. CHARA, Keck, VLTI; McAlister et al. 1994, Colavita et al. 1998, Mariotti et al. 1998) will have even larger baselines, although their larger apertures (typically 1 to 2 m, versus 12-40 cm) will allow the use of more distant stars as calibration sources. However, for those more distant stars, only limited information is available, and spectral typing, photometry, and parallaxes are all less available and less accurate. Deriving expected angular sizes, and determining the degree to which a given source is ‘unresolved’, is a greater challenge in this case. Fortunately the release of the Hipparcos catalog (Perryman et al. 1997) and the future release of the data from the 2MASS and DENIS surveys, which have limiting magnitudes of $K > 14.3$ and 13.5, respectively (Beichman et al. 1998, Epchtein 1997), will provide information on these more distant sources.

2. Selection of Unresolved Calibration Stars

At the heart of selection of unresolved sources is establishment of a criterion for ‘unresolved’. Clearly such a criterion varies with instrument - a source unresolved for a 21 m baseline in the near-IR might be well resolved at a facility with a 110 m baseline at the same wavelength, or a 38 m baseline being operated at 800 nm. A given source will be adequate as an unresolved point-source reference based upon its expected size, and the uncertainty in that expected size. Simply put, a source qualifies as ‘unresolved’ if it cannot be discerned from a point source by a given instrument. The systematic limitations of an instrument’s response generally will establish what sources are truly unresolved (see §2.2 for an explicit example.)

Sources that are distinguishable by the instrument from wholly unresolved points are also used quite commonly and shall be referred to as ‘partially resolved’ calibrators. These

sources meet the criterion of establishing the zero-point of the instrument and contribute to the zero-point error due to uncertainties in their angular size estimates at a level up to but not exceeding to the systematic error. Furthermore, sources that are even larger than this and are fully resolved by the instrument can be used to establish the zero point of the instrument, albeit at a lower degree of accuracy. These sources can be resolved stars whose angular sizes have been measured in the past, although care must be taken in using measurements from different wavelengths.

2.1. Uniform Disk Visibility

The visibility squared of a uniform disk is given as

$$V^2(x) = \left(\frac{2J_1(x)}{x} \right)^2 \tag{1}$$

where $x = \pi\theta B/\lambda_0$, and $J_1(x)$ is the first order Bessel function. Given an interferometer baseline B , wavelength λ_0 , and stellar angular size θ , an expected V^2 can be determined; or conversely, a measured V^2 and telescope parameters can deliver a uniform disk angular size. Stars are of course not uniform disks, but rather, limb-darkened or limb-brightened disks. These effects and their degree are wavelength-dependent. Fortunately, at $2.2 \mu\text{m}$, the effect of limb-darkening is quite small; modelling of these effects indicates it to be a $\approx 2\%$ effect for giant stars (cf. Scholz & Takeda 1987, Dyck et al. 1996a), and these models are supported by observational evidence (cf. Tuthill 1994, Dyck et al. 1998b). At shorter wavelengths and for more evolved stars (carbon stars, Mira variables), the effects become more pronounced (cf. Scholz & Takeda 1987, van Belle et al. 1997) and need to be carefully considered.

2.2. Example of Unresolved Source Selection

From the limiting night-to-night repeatability for PTI of $\Delta V^2 = 0.018$ for a recent experiment (van Belle et al. 1999), it is sensible to match the zero-point uncertainty to this limiting ΔV^2 . Assuming that for any given star we can know its angular size to a relative error of 17% (see §3.5, for example), a 0.60 milliarcsecond (mas) star will have an uncertainty of 0.102 mas with an expected V^2 of 0.949 with $\Delta V^2 = 0.018$. Actually observing this source might result in a measured V^2 of 0.80 ± 0.04 , typical for a single 120 second scan at PTI in nominal observing seeing conditions. The resultant normalization factor would be 1.16 ± 0.06 for that scan. Multiple observations of a given calibrator/target set can reduce the statistical uncertainty to the systematic limit set by the night-to-night repeatability and the calibrator angular size uncertainty. Given the $\Delta V^2 = 0.018$ uncertainty limitation, Table 1 lists estimated angular sizes and their associated acceptable error bars.

EDITOR: PLACE TABLE 1 HERE.

3. Estimation of Stellar Angular Sizes

Given that a desired expected angular size and its associated uncertainty have been established, the next step is to derive those angular sizes. A number of tools are at our disposal. First, linear radius can be used in conjunction with distance to estimate angular size. Second, under the assumption of black body behavior, wide-band photometry fitted to a Planck function can also deliver angular sizes. Third, use of existing angular sizes can be used to establish a relationship between $V - K$ and $B - K$ colors, and $V = 0$ and $B = 0$ apparent angular sizes.

3.1. Angular Size References in the Literature

As a test of the methods discussed, we shall be examining the predictions of the various estimators against known angular diameters. For stars that have evolved off of the main sequence, angular diameters as determined in the near-infrared are preferred, as limb darkening - and the need for models to compensate for it - is less than at shorter wavelengths. There are four primary sources in the literature of near-infrared angular diameters (primarily K band):

Kitt Peak. The lunar occultation papers by Ridgway and his coworkers (Ridgway et al. 1977a, 1977b, 1979, 1980a, 1980b, 1982a, 1982b, 1982c, Schmidtke et al. 1986) established the field of measuring angular sizes of cool stars in the near-infrared. This effort is no longer active.

TIRGO. The lunar occultation papers by Richichi and his coworkers (Richichi et al. 1988, 1991, 1992a, 1992b, 1995, 1998a, 1998b, 1998c, 1998d, Di Giacomo et al. 1991) have further developed this particular technique of diameter determinations. The group is continuing to explore the high-resolution data obtainable from lunar occultations. The recent publications from the TIRGO group include data from medium to large aperture telescopes (1.23m - 3.5m), along with concurrent photometry.

IOTA. The K band angular diameters papers from the Infrared-Optical Telescope Array by Dyck and his coworkers (Dyck et al. 1996a, 1996b, 1998b, van Belle et al. 1996, 1997, van Belle & Thompson 1999) provided a body of information on normal giant and supergiant papers, and also on more evolved sources such as carbon stars and Mira variables. Recently, results from this interferometer using the FLUOR instrument have become available (Perrin et al. 1998).

PTI. Although there is only one angular diameter paper currently available from the Palomar Testbed Interferometer (van Belle et al. 1999), 69 objects are presented in the manuscript from this highly automated instrument.

Altogether, this collection from the literature represents 92 angular diameters for 67 carbon stars and Miras, and 197 angular diameters for 190 giant and supergiant stars. In addition to these near-infrared observations, shorter wavelength observations were used to obtain diameters for main sequence objects – few near infrared observations exist for these smaller sources. These objects were culled from the catalog by Fracassini et al. (1988), limiting the investigation to direct angular size measures found in that catalog: lunar occultations, eclipsing and spectroscopic binaries, and the intensity interferometer observations of Hanbury Brown et al. (1974). Unfortunately, this sample of 50 main sequence objects is much smaller than the evolved star sample, largely reflecting the current resolution limits (roughly 1 mas) in both the interferometric and lunar occultation approaches. Furthermore, many of main sequence stars do not have sufficient photometry to be used in the techniques discussed in §3.4 and §3.5.

Shorter wavelength observations of giant and supergiant stars, while available (eg., Hutter et al. 1989, Mozurkewich et al. 1991), were not utilized in this study for two reasons. First, there are complications arising from reconciling angular diameters inferred from short wavelength ($\lambda < 1.2\mu\text{m}$) observations with the desired Rosseland mean diameters for these cooler stars. Second, the majority of the data collected on these stars, represented in the Mark III interferometer database, remains unpublished. Fortunately, these data are anticipated to be published soon (Mozurkewich 1999) and will be complimented by additional data from the NPOI interferometer (Nordgren 1999).

3.2. Error Bars and Confidence Levels

One particularly important point to note is the concept of error bars and confidence levels. The norm in the literature cited above is to quote 1σ error bars. It is equivalent to state that these error bars correspond to a single standard deviation of the data, or, under the assumption of a Gaussian distribution, that these error bars correspond to the 68% confidence level. The two and three sigma error bars correspond to the 95% and 99% confidence level, respectively.

In the interest of selecting sources, one is interested in determining *a priori* if one or more sources will be unresolved. In practice, it is often the case that multiple calibrators are initially used in an observing run, until one of the potential calibration objects has been observationally verified as actually having a visibility indistinguishable from a point source. If the predicted size for a supposed point source has only a 1σ error bar associated with it, then there is a 32% chance that the actual size will fall outside of the expected range, and as such, there is a substantial chance that the source could be unsuitable for use as a calibrator.

The errors quoted in this paper will be given as errors relative to the primary value. For example, if the 2σ error bar for a given method is cited as a 20% error bar, then a prediction of 3 mas from that method will have a 0.6 mas error, with 95% of measured values between 2.4 and 3.6 mas.

Under the assumption that out of multiple calibrators, a single good calibrator can be used to disqualify poor calibrators, one approach is to utilize numerous sources with less confidence associated with their size. In Table 2, the confidence levels associated with 1, 2, and 3σ error bars is listed, along with the probability P of not finding a single suitable calibrator when multiple stars are used for each confidence level. For a 0.3% probability that the selected calibrators are not the size expected (corresponding to the loss of one

observation set in 300 due to improper calibration), 2 or more calibrators with at least a 2σ error associated with their size are required.

EDITOR: PLACE TABLE 2 HERE.

3.3. Linear Radius

Based upon the distance to a star and its expected linear radius, an angular size can be derived. The relationships between angular diameter θ (mas), linear radius R (R_\odot), parallax π (mas), and distance d (pc) are:

$$\theta = 2 \times R \times 6.96 \cdot 10^8 \frac{\text{m}}{R_\odot} \times \left(d \times 3.09 \cdot 10^{16} \frac{\text{m}}{\text{pc}} \right)^{-1} \times 206265000 \frac{\text{mas}}{\text{rad}} \quad (2)$$

$$= 9.292 \times \frac{R}{d} \quad (3)$$

$$= 0.009292 \times R\pi \quad (4)$$

Note that the convention in the literature is for linear radius and angular diameter - conversions from linear radii to angular diameters often have an overlooked factor of 2. This approach to determine angular size is the most straightforward, assuming one can provide realistic values for R and d (or π), and their uncertainties.

The primary sources for stellar distances is the Hipparcos catalog (Perryman et al. 1997), which includes parallaxes for 118,000 stars out to 1 kpc. The catalog’s accuracy for parallaxes is 1 mas; for distances accurate to 30%, we would usually limit use of parallaxes to those that indicate distances of 300 pc or less.

Linear Radius by Spectral Type: Main Sequence Stars. Using the main sequence stars noted in §3.1, a mean radius-spectral type relationship is found for these objects:

$$R = 1.21 \pm 0.22 + 1.47 \pm 0.38 \cdot 10^6 \times SP^{-4.17 \pm 0.07} R_\odot, \quad (5)$$

for B0 (SP=20) through G3 (SP=53). The errors on the 3 parameters in the equation above are 1σ errors determined from a χ^2 minimization. Given 3 degrees of freedom in the equation, $\Delta\chi^2 = 3.53$ about the χ^2 minimum for this case (Press et al. 1992). Similar error calculations will be given for all other relationships reported in this manuscript. Strictly comparing the predictions with the measured radius values, size predictions had 1, 2, and 3σ errors (68%, 95%, 99% confidence levels) corresponding to 25%, 42% and 60%, respectively. The size of these error bars is an indicator of two aspects of spectral typing in this application: first, it is often not accurately or consistently done (particularly with regards to determination of luminosity class along with spectral type), and second, it is not particularly adequate as a single parameterization for deriving radius.

Linear Radius by Spectral Type: Giant Stars. From van Belle et al. (1999), the empirical relationship based upon 95 luminosity class III stars is:

$$R = 4.04 \pm 1.40 + 9.58 \pm 0.84 \cdot 10^{0.096 \pm 0.006 \times (SP - 60)} R_{\odot}, \quad (6)$$

where $SP = 57, \dots, 65, 66, \dots, 72$ for spectral types G7, ..., K5, M0, ..., M6. For the fit, the 1, 2, and 3σ errors are 22%, 37%, and 52%, respectively, for a given value of R .

Linear Radius by $V - K$ Color: Main Sequence Stars. No clear correlation is seen between $V - K$ color and main sequence star linear diameters. This is consistent with both bandpasses being on the Rayleigh-Jeans tail of the Planck function for most of these hot ($T > 5000\text{K}$) stars.

Linear Radius by $V - K$ Color: Giant Stars. In addition to the linear radius - spectral type relationship found in van Belle et al. (1999), an empirical relationship for linear radius as a function of $V - K$ color is also given. For the range of $V - K$ from 2.0 to 6.0, linear radius is given by:

$$R = 1.76 \pm 0.13 \times (V - K)^{2.36 \pm 0.06} R_{\odot}; \quad (7)$$

the average absolute deviation over that range is 22%, and the 2 and 3σ error bars are 36%

and 51%, respectively, for a given value of R .

3.4. Bolometric Flux

Fitting a Planck curve to wide-band photometry can lead to an estimate of temperature and angular size. Considerable photometry exists for many stars at B through K (and longer wavelengths), which can be readily accessed over the Internet (see §3.4.2). Many, though certainly not all, stars are adequately characterized as black-body radiators (BBR) for the purposes of this paper. More detailed photometric and spectrophotometric methods provide results with greater accuracy (1-2% diameters; cf. Blackwell & Lynas-Gray 1998, Cohen et al. 1996), but diameters from these methods are available for a limited number of objects.

At the low end of the temperature scale, stars down to 3500K do not depart from BBR behavior significantly. Below this temperature, stars are departing from BBR behavior due to molecular absorption in their atmospheres and mass loss processes. At the high end of the temperature scale, stars with temperatures up to roughly 7000K do not depart from BBR behavior significantly. Since results on the hotter stars depend more heavily upon the short wavelengths, both adequate corrections for reddening and short wavelength atmospheric effects such as the Balmer discontinuity become much more important. Beyond 7000K, stars are beginning to depart from BBR behavior due to the onset of non-gray opacity effects.

Although the actual computations to obtain an angular size estimate from photometric data is more challenging than from the linear radius method, the results tend to be somewhat better.

3.4.1. BBR Fit Validity

Main Sequence Stars. Main sequence stars between B and G spectral types are ideal calibrators when *BVRIJHK* photometry is available. From the culled Fracassini catalog (1988), there are 39 main sequence stars with sufficient photometry to determine a blackbody fit and corresponding angular size θ_{BBR} ; these objects were of spectral types B, A, F, and G. For the 20 larger objects with $\theta_{ACTUAL} > 0.3$ mas, the corresponding relationship between blackbody diameters and measured diameters was determined as:

$$\theta_{MEASURED} = -0.005 \pm 0.175 + 0.999 \pm 0.147 \times \theta_{BBR}. \quad (8)$$

The 1, 2 and 3σ relative error bars for this sample are 27%, 54% and 81%, respectively. For the whole sample of 39 stars, the fit was:

$$\theta_{MEASURED} = -0.093 \pm 0.165 + 1.042 \pm 0.171 \times \theta_{BBR}. \quad (9)$$

The 1, 2 and 3σ relative error bars for this sample are 41%, 81% and 121%, respectively, when the above fit is used to de-trend the data.

As suggested above, the reason that stars with smaller angular extent are being overestimated in size by a blackbody fit is most likely either insufficiently-corrected interstellar extinction, or short wavelength non-grey opacity effects. The smaller stars tend to be either hotter or more distant objects, or both. Although the fits noted above were adjusted for interstellar extinction based upon the Hipparcos parallax, if any residual reddening were present in the data, there would be a tendency for the blackbody fits to appear cooler and larger. Flux depressions of 5-10% in the 0.4-0.5 μm bandpasses, with none in the $\lambda > 1.0\mu\text{m}$ bandpasses (corresponding roughly to the perceived effects of interstellar extinction) would make the blackbody fit for a 15,000K star appear to be 14,000K, with a 10% increase in size. Furthermore, the growing effect of the Balmer discontinuity for stars with $T_{EFF} > 7,000\text{K}$ make the BBR approach highly questionable for the hotter stars.

Giant and Supergiant Stars. There is a general tendency for blackbody fits to overestimate the sizes of giant and supergiant stars. This tendency does not appear to be any more severe for luminosity class I and II stars versus giants, but does appear to become more aggravated as blackbody fits are performed on later spectral types. The data for BBR predicted and measured angular sizes can be seen in Figure 1. The parameters for the linear relationship between predicted size and actual measured size can be see in Table 3. These parameters were determined for both photometrically well-sampled stars, and for stars with poor photometric coverage; the outcomes do not appear to vary greatly.

EDITOR: PLACE TABLE 3 HERE.

EDITOR: PLACE FIGURE 1 HERE.

Also given in Table 3 is the ratio between blackbody fit diameters and measured diameters. As can be seen for the F and G class giant and supergiant subset, the departure from blackbody behavior is not statistically significant; for the K class objects, the departure is beginning to manifest itself but is only a $\approx 15\%$ effect at the 1σ level. For the M class objects, the effect is larger, but with a great deal of spread; the roughly $\approx 60\%$ effect has a standard deviation of 40-60%, depending upon the sample cut.

Finally, Table 3 presents the 1, 2, and 3σ relative errors associated with the various samples. These relative errors were obtained for angular sizes obtained from bolometric flux fits, and then adjusted according to the slope and intercepts given in the table. Consistent with this discussion is the result that the F, G, and K type stars have relatively little spread when compared to the M type stars. Also apparent from the relative errors is the slight improvement in size prediction for those stars where large amounts of photometry exists.

3.4.2. Sources of Photometry on the Internet

General Data. One of the more thorough references on stellar objects is SIMBAD (<http://simbad.u-strasbg.fr/> (France) and <http://simbad.harvard.edu/> (US Mirror)). In addition to the web-based query forms, one may also obtain information from SIMBAD by telnet and email. It is important to note that SIMBAD is merely a clearing house of information from a wide variety of sources and is not an original source in and of itself; any information that ends up being crucial to the merit of an astrophysical investigation should be checked against its primary source.

Infrared Photometry ($\lambda > 1\mu m$). The Catalog of Infrared Observations (CIO), a extensive collection of IR photometry by Gezari et al. (1993) has been updated, although the most recent version is available only online (Gezari, Pitts & Schmitz 1997). The latter catalog can be queried with individual stars or lists of objects at VizieR (<http://vizier.u-strasbg.fr/> (France) and <http://adc.gsfc.nasa.gov/viz-bin/VizieR> (US Mirror)). As with the SIMBAD data, the CIO is merely a collection of the data in the literature, and examination of the primary sources is advised. Also, as noted in the introduction, the forthcoming release of the 2MASS and DENIS catalogs will greatly augment the collective database of near-infrared photometry.

Visual Photometry. The General Catalog of Photometric Data (GCPD) provides a large variety of wide- to narrow-band visual photometry at <http://obswww.unige.ch/gcpd/gcpd.html>. For variable stars, the AAVSO and AFOEV are both excellent sources of epoch-specific V band photometry.

3.5. Apparent Angular Size versus $V - K$, $B - K$ Colors

The large body of available angular sizes allows for directly inferring expected angular sizes, bypassing considerations of stellar distance, spectral type, reddening, and linear size. To compare angular sizes of stars at different distances, one approach is to scale the sizes relative to a value of $V = 0$:

$$\theta_{V=0} = \theta \times 10^{V/5}. \quad (10)$$

The angular size thus is scaled to a constant brightness distance and becomes a measure of apparent surface brightness. Conversion between a $V = 0$ apparent angular size and actual apparent angular size is trivial with a known V magnitude and the equation above; the same approach can be employed for $K = 0$ (see Dyck et al. 1996a) or $B = 0$. Given the general prevalence of V band and the inclusion of B band data in the 2MASS catalog, the apparent angular size approach will be developed here for $V - K$ and $B - K$ colors.

Giant and Supergiant Stars. By examining the $2.2 \mu\text{m}$ angular sizes for the 164 normal giant and supergiant stars found in the interferometry and lunar occultation papers, we can establish a relationship between $V = 0$ apparent angular size and $V - K$ color:

$$\theta_{V=0} = 10^{0.682 \pm 0.014 + 0.222 \pm 0.003 \times (V-K)}. \quad (11)$$

The 1, 2, and 3σ errors from the average absolute deviations of measured values from the fit correspond to 10%, 17% and 25%. Similarly, for $B - K$ color, 137 giant and supergiant stars had available photometry, resulting in the following fit:

$$\theta_{B=0} = 10^{0.656 \pm 0.023 + 0.220 \pm 0.004 \times (B-K)}, \quad (12)$$

with 1, 2, and 3σ errors of 9.4%, 16% and 22%.

The relationship appears valid over a $V - K$ range of 2.0 to 8.0. Blueward of $V - K = 2.0$, the subsample is too small ($N = 3$) to confidently indicate whether or not

the fit is valid, in spite of the goodness of fit for the whole subsample. The same is true redward of $V - K = 8.0$. Also, for stars redward of approximately $V - K = 8$, care must be taken to exclude variable stars (both semiregular and Miras). The data points and the fit noted above may be seen in Figure 2; $\theta_{V=0}$ and standard deviation by $V - K$ bin is given in Table 4. The Miras are plotted separately in Figure 3 and will be discussed below.

EDITOR: PLACE TABLE 4 HERE.

EDITOR: PLACE FIGURE 2 HERE.

EDITOR: PLACE FIGURE 3 HERE.

For $B - K$ between 3.0 and 7.5, the relationship appears exhibits a similar if not slightly superior validity. As with the $V - K$ color, the relationship appears to be valid down blueward of the short edge of that range, down to $B - K = -1$, but the data are sparse. Redward of $B - K = 7.5$, the relationship also exhibits potential confusion with the Mira variable stars, although there appears to be less degeneracy, but this is possibly due to a lesser availability of B band data on these very red sources. The data points and the fit noted above may be seen in Figure 4; $\theta_{B=0}$ and standard deviation by $B - K$ bin is given in Table 5.

EDITOR: PLACE TABLE 5 HERE.

EDITOR: PLACE FIGURE 4 HERE.

The potential misclassification of more evolved sources such as carbon stars and variables (Miras or otherwise) as normal giant and supergiant stars is a significant secondary consideration. For the dimmer sources for which little data is available, non-classification is perhaps the more appropriate term. What is reassuring with regards to the issue of classification errors is the fact that the robust relationships between $(\theta_{V=0}, V - K)$ and $(\theta_{B=0}, B - K)$ is valid for stars of luminosity class I, II, and III. Our experience with the available data is that errors exist more frequently in luminosity classifications rather than in typing by chemical abundance or variability. However, since the $\theta_{V=0}$ and $\theta_{B=0}$ relationships are insensitive to errors in luminosity class, this method is more robust than the linear radius-distance method, particularly for those stars in the $2.0 < V - K < 6.0$ and $3.0 < B - K < 7.5$ ranges, where few if any stars of significant variability exist. This relationship is also easier to employ than the method of BBR fits.

Evolved Sources: Variable Stars. By examining the $2.2 \mu\text{m}$ angular sizes for the 87 observations of 65 semiregular variables, Mira variables and carbon stars (broadly classified here as ‘variable stars’) found in the literature, we can establish a relationship between $V = 0$ apparent angular size and $V - K$ color:

$$\theta_{V=0} = 10^{0.801 \pm 0.039 + 0.220 \pm 0.005 \times (V - K)}. \quad (13)$$

The 1, 2, and 3σ relative errors associated with this fit are 21%, 38%, and 54%, respectively. The data points and the fit noted above may be seen in Figure 3. Similarly, for $B - K$ color, 19 evolved sources had available photometry for 29 angular size observations, resulting in the following fit:

$$\theta_{B=0} = 10^{0.878 \pm 0.065 + 0.209 \pm 0.006 \times (B - K)}, \quad (14)$$

with 1, 2, and 3σ errors of 17%, 31% and 45%.

For the variable stars, the relationship appears valid over a $V - K$, $B - K$ ranges of 5.5 to 13.0 and 9.0 to 16.0, respectively. Redward of $V - K = 13$, the sample is too small

($N = 3$) to confidently indicate whether or not the fit is valid, in spite of the goodness of fit for the general sample. It is interesting to note that the slope of the fits for the variable stars and for the giant/supergiant stars is statistically identical for both $V - K$ and $B - K$ colors; only the intercepts are different. This corresponds to a $\theta_{V=0}$ size factor of 1.40 ± 0.15 between the smaller normal and the larger variable stars for a given $V - K$ color, and a corresponding $\theta_{B=0}$ size factor of 1.34 ± 0.21 .

Main Sequence Stars. By examining the objects in the Fracassini catalog (1988; specifically, many objects from Hanbury Brown et al. 1974), there appears to be similar relationships between the $V - K$ & $B - K$ colors, and $\theta_{V=0}$ & $\theta_{B=0}$ angular sizes. However, the sample set of stars with adequate photometry is unfortunately limited, and drawing broad conclusions from the sample is potentially suspect. In the narrow ranges of $-0.5 < V - K < +0.5$ and $-0.5 < B - K < +0.5$, which are well sampled, the relationships between the colors and their apparent angular sizes are

$$\theta_{V=0} = 10^{0.503 \pm 0.027 + 0.328 \pm 0.166 \times (V-K)}, \quad (15)$$

$$\theta_{B=0} = 10^{0.502 \pm 0.017 + 0.284 \pm 0.066 \times (B-K)}. \quad (16)$$

The resulting 1,2, and 3 σ error bars are only 1.6%, 3.2%, and 4.8% for $V - K$, and 1.4%, 3.0%, and 4.6% for $B - K$. The $\theta_{V=0}$ versus $V - K$ data for these objects are plotted in Figure 5. Clearly, the relationship appears to not only hold for the B and A type objects in the $-0.5 < V - K < +0.5$ range, but also for the two G type stars seen at $V - K \approx 1.5$. Unfortunately, due to the limited sampling of the B, A, G type relationship, it is unclear how well the relationship noted in the equation above holds in the $0.5 < V - K < 1.5$ range. For the cooler K and M type stars, at $V - K > 1.5$, the relationship clearly shifts just as with the normal giant/supergiants and the variables, but towards a smaller, rather than larger apparent angular size. The intercept shifts from 0.503 to roughly 0.100, but there are again only a few (4) stars to support this observation. Similar trends are seen in

the $B - K$ data.

EDITOR: PLACE FIGURE 5 HERE.

3.6. Comparison of the Various Methods

The methods examined in this paper for establishing a calibration for an interferometer zero-point are summarized in Table 6. For main sequence stars, establishing a $\theta_{V=0}$ or $\theta_{B=0}$ apparent angular size delivers the best results (§3.5), but has only been established over narrow ranges ($-0.5 < V - K < +0.5$ and $-0.5 < B - K < +0.5$) due to limited sampling. For giant and supergiant stars, the approaches of most general validity are the angular sizes predicted by $\theta_{V=0}$ or $\theta_{B=0}$ apparent angular size (§3.5), and angular size by blackbody fit for F, G, K giants and supergiants (§3.4).

EDITOR: PLACE TABLE 6 HERE.

4. Proximity Considerations

A vital concern in the selection of calibration sources for science targets is proximity – both spatial and temporal. Variability of both the atmosphere and instrument response with pointing and time can reduce or even eliminate the correlation between system performance for the calibration source and science target. The magnitude and nature of these effects are dependent upon both the particular interferometer, the general nature of the atmospheric performance at the site, and the specific behavior of the atmosphere for a given evening of observing. These concerns are unsurprising, given the parallels of

photometry via the use of standard stars. Our experience with PTI indicates that the best results for typical observing nights occur with calibration stars within $\approx 15^\circ$ and ± 1 hour from the science targets (Boden et al. 1998), and there is an improvement in calibration accuracy as the proximity is increased, most significantly with spatial proximity. Similar evidence exists for the IOTA interferometer, although it is not as well quantified (Dyck et al. 1996a); nevertheless, the selection of calibration sources for IOTA employed similar restrictions. For the Mark III interferometer, the proximity considerations were not as significant, although the users of that particular instrument clearly took care in quantifying that particular aspect of the instrument (Mozurkewich et al. 1991).

Obviously it is prudent to understand the response of one’s instrument with regards to these considerations. Specific investigation of the correlation of system response between point-like calibration sources in a variety of circumstances is necessary to give a measure of confidence to results from interferometric instruments, particularly the error bars. Although the necessity of such quantification should be obvious, the use of merely anecdotal evidence in this regard can lead researchers to erroneous conclusions.

5. Conclusion

Clearly the use of expected angular sizes to calibrate interferometric data is a task that must be embarked upon with great care. The use of measured sizes to rigorously quantify the accepted methods of the past, and to explore potential new techniques, is a possibility only now available to the community with the large numbers of angular sizes becoming available in the literature. The approach of establishing the apparent $\theta_{V=0}$ and $\theta_{B=0}$ angular sizes appears to be a powerful tool to predict the angular sizes of main sequence and giant/supergiant stars, and to provide insight into the fundamental physical differences between giants/supergiants, and more evolved variables.

Part of the work described in this paper was performed at the Jet Propulsion Laboratory, California Institute of Technology under contract with the National Aeronautics and Space Administration. I would like to thank Andy Boden, Mark Colavita, Mel Dyck, Steve Ridgway, and Bob Thompson for valuable feedback during the development of this manuscript. This research has made use of the SIMBAD, VizieR, and AFOEV databases, operated by the CDS, Strasbourg, France. In this research, we have used, and acknowledge with thanks, data from the AAVSO International Database, based on observations submitted to the AAVSO by variable star observers worldwide.

REFERENCES

- Baldwin, J.E., et al., 1996, *A&A*, 306, L13.
- Barnes, T.G., Evans, D.S., 1976, *MNRAS*, 174, 489.
- Barnes, T.G., Evans, D.S., Parsons, S.B., 1976, *MNRAS*, 174, 503.
- Barnes, T.G., Evans, D.S., Moffett, T.J., 1978, *MNRAS*, 183, 285.
- Beichman, C.A., Chester, T.J., Skrutskie, M., Low, F.J., Gillett, F., 1998, *PASP*, 110, 480.
- Benson, J.A., Dyck, H.M., Ridgway, S.T., Dixon, D.J., Mason, W.L., Howell, R.R., 1991, *AJ*, 102, 2091.
- Blackwell, D.E., & Lynas-Gray, A.E., 1998, *A&AS*, 129, 505.
- Cohen, M., Witteborn, F.C., Carbon, D.F., Davies, J.K., Wooden, D.H., Bregman, J.D., 1996, *AJ*, 112, 2274.
- Colavita, M.M. et al., 1998, *Astronomical Interferometry*, R.D. Reasenberg, ed., *Proc. SPIE*, 3350, 776.
- Colavita, M.M. et al., 1999, *ApJ*, 510, 505.
- Di Benedetto, G.P. & Conti, G., 1983, *ApJ*, 268, 309.
- Di Benedetto, G.P., 1985, *A&A*, 148, 169.
- Di Benedetto, G.P., 1993, *A&A*, 270, 315.
- Di Giacomo, A., Lisi, F., Calamai, G., Richichi, A., 1991, *A&A*, 249, 397.
- Dyck, H.M., Benson, J.A., van Belle, G.T., Ridgway, S.T., 1996a, *AJ*, 111, 1705.
- Dyck, H.M., van Belle, G.T., Benson, J.A., 1996b, *AJ*, 112, 294.
- Dyck, H.M., 1998a, private communication.
- Dyck, H.M., van Belle, G.T., Thompson, R.R., 1998b, *AJ*, 116, 981.

- Epchtein, N., 1997, in *The Impact of Large Scale Near-infrared Surveys*, ed. F. Garzon, N. Epchtein, A. Omont, W.B. Burton, P. Persi, (Dordrecht: Kluwer).
- Fracassini, M., Pasinetti-Fracassini, L.E., Pastori, L., Pironi, R., 1988, *Bull. D'Inf. Cent. Donnees Stellaires*, 35, 121.
- Gezari, D.Y., Schmitz, M., Pitts, P.S., Mead, J.M., 1993, *Catalog of Infrared Observations*, 3rd Edition, NASA Reference Publication 1294.
- Gezari, D.Y., Pitts, P.S., Schmitz, M., 1997, *Catalog of Infrared Observations*, Edition 4, unpublished but available online at <http://adc.gsfc.nasa.gov/>.
- Hanbury Brown, R., Davis, J., Lake, R.J.W., Thompson, R.J., 1974, *MNRAS*, 167, 475.
- Hutter, D.J., et al., 1989, *ApJ*, 340, 1103.
- Maroitti, J.-M. et al. 1998, *Astronomical Interferometry*, R.D. Reasenberg, ed., *Proc. SPIE*, 3350, 800.
- McAlister, H.A., Bagnuolo, B.G., ten Brummelaar, T., Hartkopf, W. I., Turner, N. H., Garrison, A.K., Robinson, B.G., Ridgway, S.T., 1994, *Amplitude and Intensity Spatial Interferometry II*, James B. Breckinridge, Ed., *Proc. SPIE*, 2200, 129.
- Mozurkewich, D., Johnston, K. J., Simon, Richard S., Bowers, P. F., Gaume, Ralph, Hutter, D. J., Colavita, M. M., Shao, M., Pan, X. P. 1991, *AJ*, 101, 2207.
- Mozurkewich, D., 1999, private communication.
- Nordgren, T., 1999, private communication.
- Press, W.H., Teukolsky, S.A., Vetterling, W.T., Flannery, B.P., 1992, *Numerical Recipes in C* (Port Chester, NY: Cambridge University Press), 689.
- Perrin, G., Coud du Foresto, V., Ridgway, S.T., Mariotti, J.-M., Traub, W.A., Carleton, N.P., Lacasse, M.G., 1998, *A&A*, 331, 619.

- Perryman, M. A. C., Lindegren, L., Kovalevsky, J., Hog, E., Bastian, U., Bernacca, P. L., Creze, M., Donati, F., Grenon, M., Grewing, M., Van Leeuwen, F., Van Der Marel, H., Mignard, F., Murray, C. A., Le Poole, R. S., Schrijver, H., Turon, C., Arenou, F., Froeschle, M., Petersen, C. S., 1997, *A&A*, 323, L49.
- Richichi, A., Salnari, P., Lisi, F., 1988, *ApJ*, 326, 791.
- Richichi, A., Lisi, F., Calamai, G., 1991, *A&A*, 241, 131.
- Richichi, A., Lisi, F., Di Giacomo, A., 1992, *A&A*, 254, 149.
- Richichi, A., Di Giacomo, A., Lisi, F., Calamai, G., 1992, *A&A*, 265, 535.
- Richichi, A., Chandrasekhar, T., Lisi, F., Howell, R.R., Meyer, F., Rabbia, Y., Ragland, S., Ashok, N.M., 1995, *A&A*, 301, 439.
- Richichi, A., Ragland, S., Fabbroni, L., 1998a, *A&A*, 330, 578.
- Richichi, A., Stecklum, B., Herbst, T.M., Lagage, P.-O., Thamm, E., 1998b, *A&A*, 334, 585.
- Richichi, A., Ragland, S., Stecklum, B., Leinert, C., 1998c, *A&A*, 338, 527.
- Richichi, A., et al. 1998d, (in preparation).
- Ridgway, S.T., Jacoby, G.H., Joyce, R.R., Wells, D.C., 1980, *AJ*, 85, 1496.
- Ridgway, S.T., Wells, D.C., Joyce, R.R., 1977, *AJ*, 82, 414.
- Scholz, M., Takeda, Y., 1987, *A&A*, 186, 200.
- Tuthill, P.G., 1994, PhD Dissertation, University of Cambridge.
- van Belle, G.T., Dyck, H.M., Benson, J.A., Lacasse, M.G., 1996, *AJ*, 112, 2147.
- van Belle, G.T., Dyck, H.M., Thompson, R.R., Benson, J.A., Kannappan, S.J., 1997, *AJ*, 114, 2150.
- van Belle, G.T., et al., 1999a, *AJ*, 117, 521.

van Belle, G.T., Thompson, R.R., 1999, in preparation.

Table 1. Allowable Errors in Angular Size

Estimated Angular Size (mas)	Expected V^2
0.100±0.271	0.999±0.018
0.200±0.210	0.994±0.018
0.300±0.168	0.987±0.018
0.400±0.138	0.977±0.018
0.500±0.117	0.964±0.018
0.600±0.102	0.949±0.018
0.700±0.091	0.931±0.018
0.800±0.082	0.911±0.018

Table 2. Probability of 1 or More Stars not within Expected Size Range

σ	Confidence	Probability P		
	Level	1 star	2 stars	3 stars
1	0.68	0.32	0.10	0.03
2	0.95	0.05	0.003	0.0001
3	0.99	0.01	0.0001	10^{-6}

Table 3. Linear Relationship between Blackbody and Actual Angular Sizes

Spectral Types	Luminosity		N	Slope		Intercept			
	Class	DOF		b	a	Ratio	1σ	2σ	3σ
All	All	> 3	201	0.69	0.47	1.45 ± 0.53	0.182	0.35	0.517
FG	All	> 15	9	0.79	0.43	1.00 ± 0.14	0.072	0.125	0.177
K	All	> 15	30	0.76	0.43	1.17 ± 0.14	0.081	0.148	0.215
M	All	> 15	46	0.63	0.63	1.59 ± 0.38	0.2	0.393	0.585
FG	All	> 3	14	0.86	0.22	1.02 ± 0.14	0.08	0.156	0.232
K	All	> 3	52	0.78	0.29	1.15 ± 0.30	0.095	0.174	0.252
M	All	> 3	132	0.57	0.52	1.62 ± 0.55	0.21	0.448	0.687
M	III	> 15	35	0.55	1.54	1.60 ± 0.41	0.19	0.386	0.581
M	III	> 3	113	0.6	0.61	1.62 ± 0.57	0.232	0.521	0.809

Note. — Linear relationship $\theta_{ACTUAL} = a + b \times \theta_{BBR}$ between blackbody and actual angular sizes for luminosity class I, II and III oxygen-rich stars. DOF is the number of photometry data point degrees of freedom for the blackbody fits; N is the number of stars available for each subset. Ratio is the average value of $\theta_{BBR}/\theta_{ACTUAL}$ for each subset. The error bars given are for the average relative difference between θ_{ACTUAL} and θ'_{BBR} , where θ'_{BBR} is θ_{BBR} detrended using the linear parameters a and b such that $\theta'_{BBR}/\theta_{ACTUAL} = 1$.

Table 4. Apparent Angular Size as a Function of $V - K$ Color

$V - K$ Center	Normal Giants and Supergiants				Variables				
	N	$\bar{\theta}_{V=0}$	Std. Dev.	Fit	N	$\bar{\theta}_{V=0}$	Std. Dev.	Fit	Ratio
-0.5	1	3.4		3.7	0				
0.0	0			4.8	0				
0.5	0			6.2	0				
1.0	1	9.1		8.0	0				
1.5	2	11.6	1.8	10.3	0				
2.0	9	13.9	1.7	13.3	0				
2.5	17	16.7	3.1	17.2	0				
3.0	12	20.5	3.1	22.3	0				
3.5	20	27.2	4.4	28.7	0				
4.0	21	37.8	4.4	37.1	0				
4.5	15	47.0	5.7	47.9	0				
5.0	18	58.2	5.9	61.9	0				
5.5	15	80.3	13.9	79.9	4	105	13	103	1.31 ± 0.28
6.0	7	102.7	13.3	103.1	7	140	25	132	1.37 ± 0.30
6.5	5	122.9	18.3	133.1	9	181	57	170	1.47 ± 0.51
7.0	9	159.6	23.5	171.9	8	233	60	220	1.46 ± 0.43
7.5	6	197.0	21.0	221.9	14	270	62	283	1.37 ± 0.35
8.0	0			286.6	9	461	184	365	
8.5	1	355.4		370.0	4	605	217	470	1.70 ± 0.61
9.0	1	431.0		477.7	7	631	245	605	1.46 ± 0.57
9.5	0				3	841	259	780	
10.0	0				2	1286	511	1005	
10.5	0				4	1456	604	1295	
11.0	0				6	1795	465	1669	
11.5	0				2	2146	498	2150	
12.0	0				0				
12.5	0				2	3033	965	3569	
13.0	0				0				
13.5	0				0				
14.0	0				1	8323		7635	

Note. — The number of stars N , average size $\theta_{V=0}$, and standard deviation for each bin is given for both normal giant and supergiant stars, and for variables, inclusive of Miras, semi-regulars, and carbon stars. The fits given are those discussed in §3.5; the ratios given are the average $\theta_{V=0}$ size ratios for those $V - K$ bins where values exist for both giant/supergiant stars

Table 5. Apparent Angular Size as a Function of $B - K$ Color

$B - K$ Bin Center	Normal Giants and Supergiants				Variables				Ratio
	N	$\bar{\theta}_{B=0}$	Std. Dev.	Fit	N	$\bar{\theta}_{B=0}$	Std. Dev.	Fit	
-0.5	1	3.2		3.5	0				
0.0	0			4.5	0				
0.5	0			5.8	0				
1.0	0			7.5	0				
1.5	1	10.9		9.7	0				
2.0	1	13.6		12.5	0				
2.5	1	18.7		16.1	0				
3.0	10	21.4	2.7	20.7	0				
3.5	13	26.2	4.2	26.7	0				
4.0	11	34.5	3.6	34.4	0				
4.5	6	47.2	8.2	44.3	0				
5.0	15	51.9	5.3	57.1	0				
5.5	14	74.9	11.5	73.6	0				
6.0	18	89.5	12.0	94.8	0				
6.5	12	114.4	19.3	122.1	0				
7.0	13	151.5	15.9	157.4	0				
7.5	6	196.1	21.3	202.8	0				
8.0	4	248.4	23.2	261.2	6	304	75	352	1.23 ± 0.32
8.5	7	315.6	21.8	336.6	3	451	84	447	1.43 ± 0.28
9.0	2	344.2	5.5	433.7	1	520		569	
9.5	0				5	669	164	723	
10.0	0				3	1057	273	919	
10.5	0				1	1270		1169	
11.0	0				0				
11.5	0				2	2501	561	1889	
12.0	0				2	2802	316	2402	
12.5	0				0				
13.0	0				1	3302		3883	
13.5	0				0				
14.0	0				1	5797		6276	
14.5	0				1	9077		7979	
15.0	0				2	12161	1755	10144	

Note. — The number of stars N , average size $\theta_{B=0}$, and standard deviation for each bin is given for both normal giant and supergiant stars, and for variables, inclusive of Miras, semi-regulars, and

Table 6. Comparison of the Various Angular Size Prediction Methods

Method	1 σ	2 σ	3 σ	Notes
Linear Radius by Spectral Type				
Main Sequence Stars	25%	42%	60%	
Giant Stars	22%	37%	52%	
Linear Radius by $V - K$ Color				
Giant Stars	22%	36%	51%	
Angular Size by BBR Fit				
Main Sequence Stars	13%	35%	57%	
Giant, Supergiant Stars (all)	18%	35%	52%	
F & G Giant, Supergiant Stars	8%	16%	23%	
K Giant, Supergiant Stars	10%	17%	25%	
M Giant, Supergiant Stars	21%	45%	69%	
$V = 0$ Angular Size by $V - K$ Color				
Main Sequence Stars	1.6%	3.2%	4.8%	Limited $V - K$ range
Giant, Supergiant Stars	10%	17%	25%	
Variable Stars	21%	38%	54%	
$B = 0$ Angular Size by $B - K$ Color				
Main Sequence Stars	1.4%	3.0%	4.6%	Limited $B - K$ range
Giant, Supergiant Stars	9.4%	16%	22%	
Variable Stars	17%	31%	45%	

Note. — 1, 2, and 3 σ errors given above are percentage errors relative to the value predicted by each method.

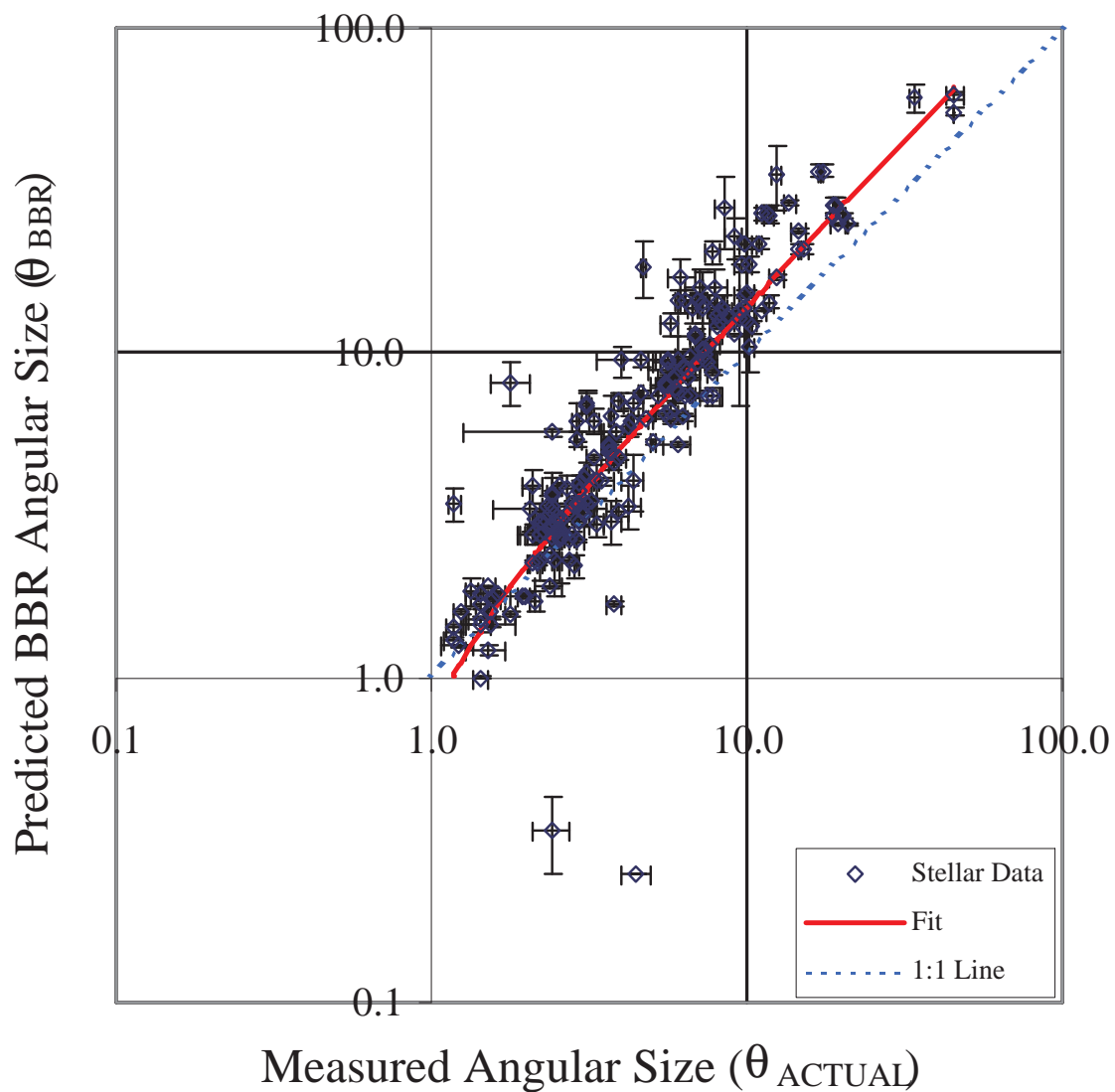


Fig. 1.— Predicted blackbody radiator (BBR) angular sizes (θ_{BBR}) versus measured angular sizes (θ_{ACTUAL}) for luminosity class I, II and III objects of all available spectral types. The BBR equals measured angular size diagonal line is also shown for comparison.

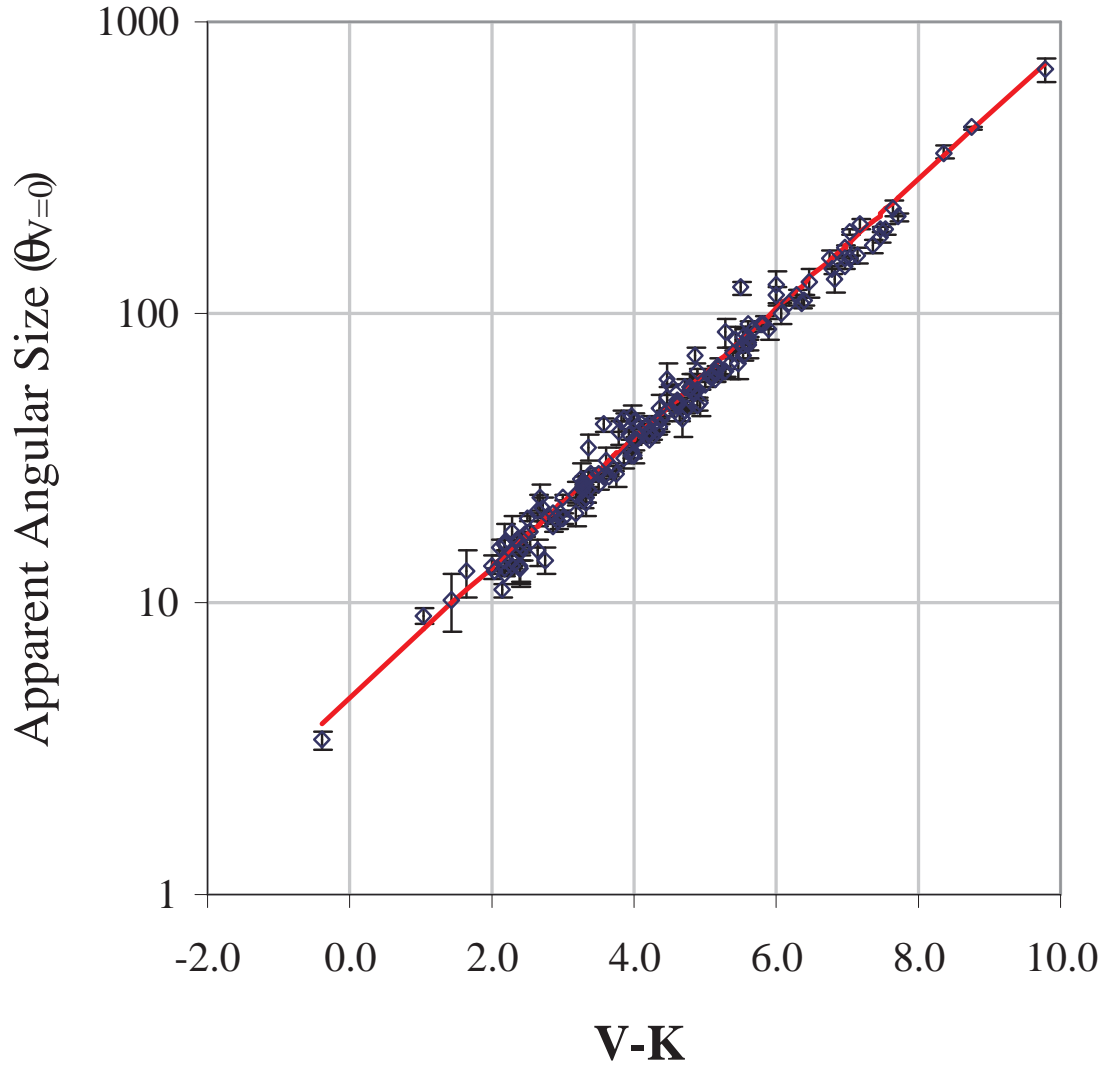


Fig. 2.— The $\theta_{V=0}$ apparent angular size versus $V - K$ color for luminosity class I, II, and III giant stars.

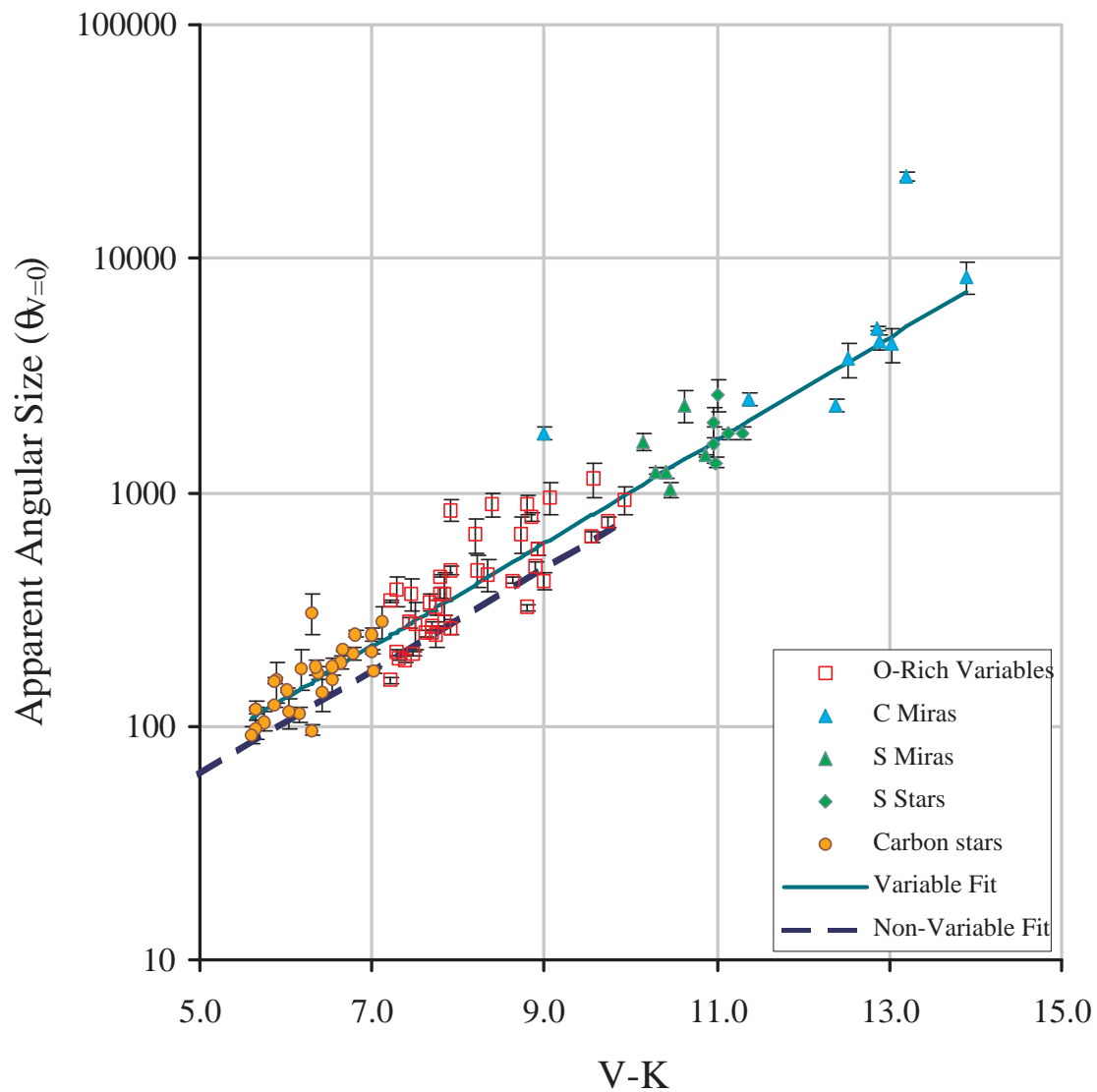


Fig. 3.— The $\theta_{V=0}$ apparent angular size versus $V - K$ color for evolved stars, including carbon stars, S stars, all types of Mira variables, and non-Mira variables. The solid upper line is the fit line for these objects, and the dashed lower line is the fit line for the giants and supergiants from Figure 2.

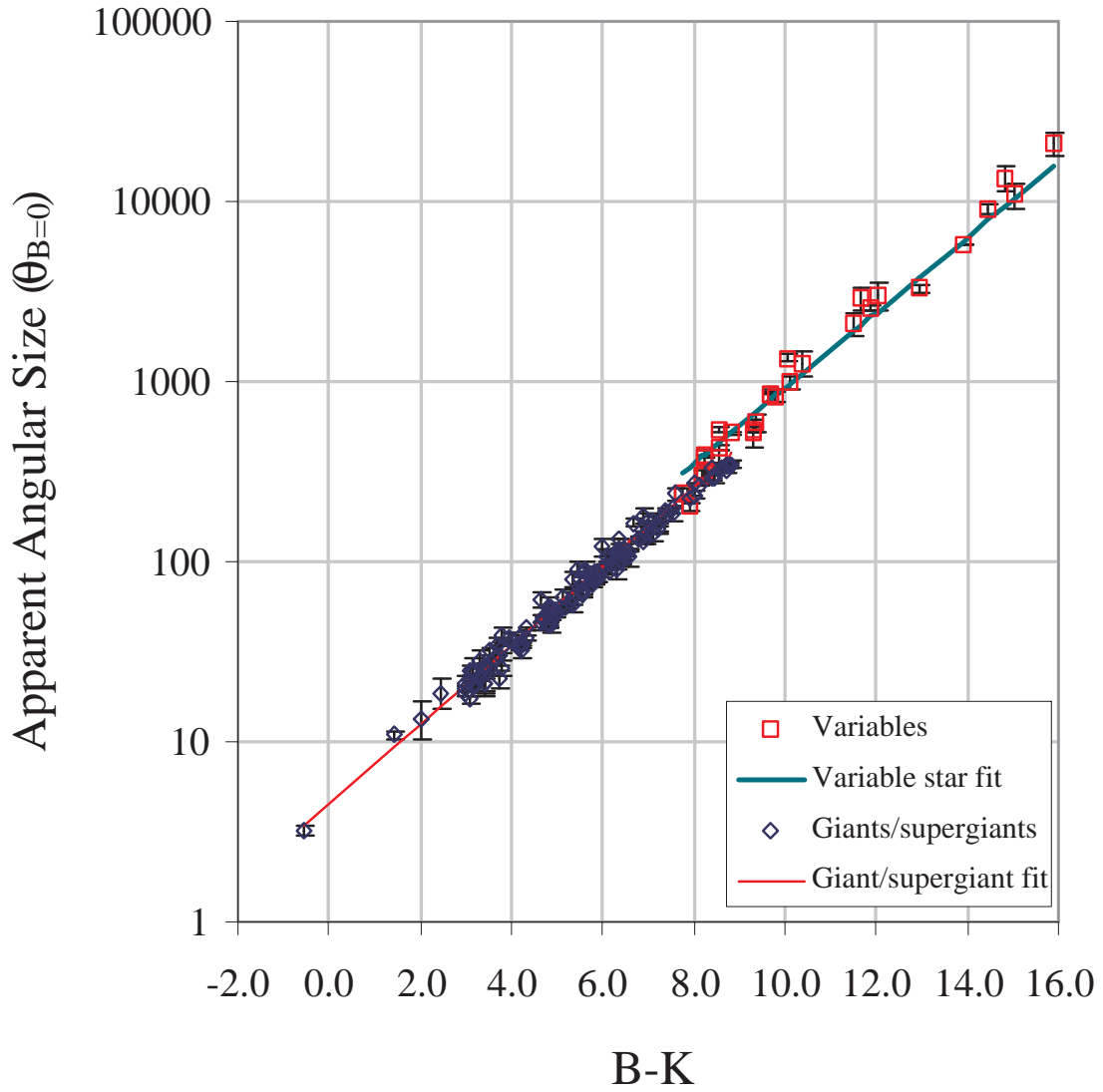


Fig. 4.— The $\theta_{B=0}$ apparent angular size versus $B - K$ color for giant/supergiant stars and evolved stars, which includes Mira variables, S stars, carbon stars, and non-Mira variables. The upper line is the fit line for the evolved stars, the lower line is the fit line for the giants and supergiants.

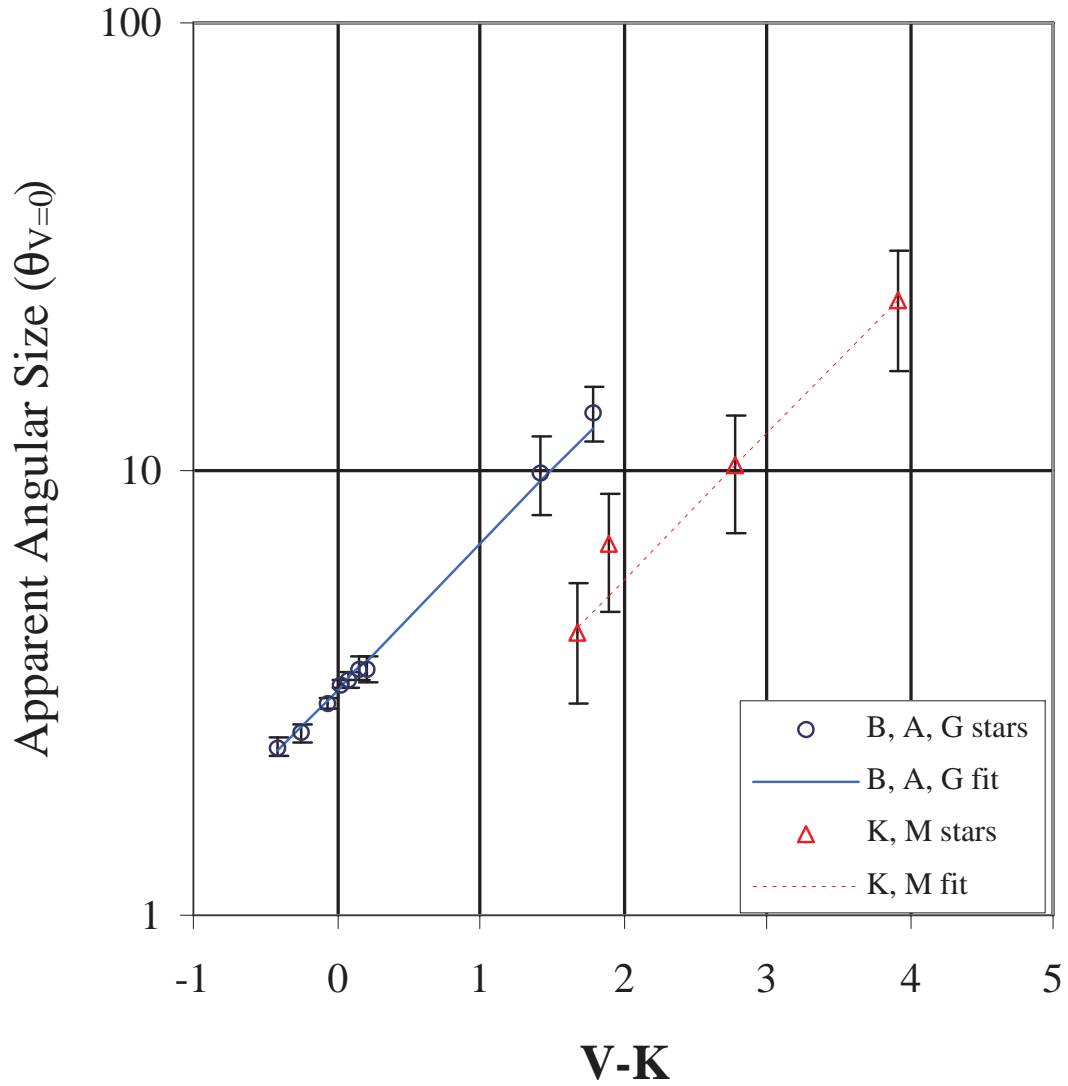


Fig. 5.— The $\theta_{V=0}$ apparent angular size versus $V - K$ color for main sequence stars. The circles and solid line are the data points and fit for B, A, and G type stars, respectively; the triangles and dotted line are the data points and fit for K, M stars, respectively.